



Full-Length Article

Targeted insights into *Aeromonas hydrophila* biofilms: Surface preferences, resistance mechanisms, and gene expression

Md. Ashikur Rahman^{a,b,e}, Shirin Akter^{a,b,f}, Md. Ashrafudoulla^{c,g}, Meidistria Tandirapak^{a,b}, Kyung Ok Lee^d, Sang-Do Ha^{a,b,*}

^a Food Safety and Regulatory Science, Chung-Ang University, Anseong-Si, Republic of Korea

^b GreenTech-based Food Safety Research Group, BK21 Four, Chung-Ang University, 4726 Seodong-daero, Anseong, Gyeonggido 17546, Republic of Korea

^c National Institute of Health, 9000 Rockville Pike, Bethesda, MD 20892, USA

^d Food Safety Division Research Institute of Food Hygiene, Hyundai green food, Yongin, Republic of Korea

^e Bangladesh Fisheries Research Institute, Mymensingh 2201, Bangladesh

^f Department of Fisheries and Marine Bioscience, Bangabandhu Sheikh Mujibur Rahman Science and Technology University, Gopalganj 8100, Bangladesh

^g Department of Food Science, Center for Food Safety, University of Arkansas System Division of Agriculture, Fayetteville, AR 72704, USA

ARTICLE INFO

Keywords:

A. hydrophila

Biofilm

Antibiotic resistance

Gene expression

Food contact surface

ABSTRACT

This study provides a comprehensive analysis of biofilm formation, antibiotic resistance, motility, and gene expression in four *Aeromonas hydrophila* strains—ATCC 15467, ATCC 7966, KCTC 2358, and KCTC 11533—on stainless steel (SS), silicon rubber (SR), polyethylene terephthalate (PET), and high-density polyethylene (HDPE) surfaces over 24, 48, 72, and 96 h. Biofilm formation peaked at 72 h, with ATCC 7966 demonstrating the highest biofilm density on PET ($6.50 \pm 0.08 \log \text{CFU/cm}^2$), underscoring PET's role as a favorable substrate for biofilm development. In contrast, HDPE consistently exhibited the lowest biofilm levels, reflecting its potential as a biofilm-resistant material. Antibiotic susceptibility profiling revealed multidrug resistance (MDR) in ATCC 15467 and KCTC 11533 (MARI = 0.80), particularly against beta-lactams, aminoglycosides, and fluoroquinolones while ATCC 7966 and KCTC 2358 displayed moderate resistance. Motility assays highlighted strain-specific capabilities, with KCTC 11533 exhibiting the highest swimming motility ($76.0 \pm 6.6 \text{ mm}$) and KCTC 2358 excelling in swarming ($47.7 \pm 3.5 \text{ mm}$). Genetic analysis confirmed the presence of *luxS* and *ahyR* in all strains, while *csgA* was exclusive to ATCC 7966, correlating with its superior biofilm formation. Confocal microscopy revealed biofilm maturation dynamics, with red fluorescence indicating cell death and aging at 96 h, while SEM images captured intricate surface-specific biofilm architectures. These findings elucidate the critical interplay between strain characteristics, surface properties, and incubation time, providing a foundation for developing targeted strategies to control *A. hydrophila* biofilms in food processing environments.

Introduction

Biofilms, intricate conglomerates of microorganisms ensconced within a self-generated extracellular matrix (ECM), pose a formidable challenge across diverse sectors, including healthcare, water systems, food production and the poultry industry (Rahman et al., 2023). These biofilms, acting as persistent reservoirs for pathogens, are resistant to cleaning and disinfection measures, posing significant threats by enabling long-term survival and dissemination of the bacterium on food contact surfaces, which can lead to contamination and outbreaks of foodborne illnesses, particularly in the food and poultry industries (Ashikur Rahman, et al., 2024; El-Hossary, et al., 2023). *Aeromonas*

hydrophila, a Gram-negative bacterium, stands out among biofilm-forming microorganisms for its remarkable adaptability and resilience, thriving in diverse ecological niches such as aquatic environments, soil, sewage, and food processing facilities, while forming tenacious biofilms on a wide range of surfaces under varied environmental conditions (Akter, et al., 2025; Grilo, et al., 2020; Rahman, et al., 2019).

In the poultry sector, *A. hydrophila* presents a dual threat. During production, it can cause localized and systemic infections in poultry, resulting in significant economic losses. Post-harvest, the bacterium contaminates carcasses and water used in processing plants, further compromising food safety. Its transmission often occurs through the

* Corresponding author.

E-mail address: sangdoha@cau.ac.kr (S.-D. Ha).

<https://doi.org/10.1016/j.psj.2025.104851>

Received 7 January 2025; Accepted 23 January 2025

Available online 25 January 2025

0032-5791/© 2025 The Authors. Published by Elsevier Inc. on behalf of Poultry Science Association Inc. This is an open access article under the CC BY-NC-ND license (<http://creativecommons.org/licenses/by-nc-nd/4.0/>).

fecal-oral route, facilitated by contaminated feed, water, or inadequate hygiene practices. Additionally, *A. hydrophila* produces a diverse array of virulence factors, including endotoxins and biofilms, which enhance its pathogenicity and persistence (Abd El-Ghany, 2023).

Therefore, deciphering the mechanisms of biofilm formation and detachment on different food contact surfaces is crucial for devising effective strategies to mitigate the risks posed by *A. hydrophila*. Biofilm formation and virulence in *A. hydrophila* are tightly controlled by several key genes, including *luxS*, *ahyR*, and *csgA*. The *luxS* gene is responsible for the production of autoinducer-2 (AI-2), a crucial signaling molecule in the quorum sensing (QS) system, which enables bacterial communication and coordination of biofilm development, virulence factor production, and adaptation to environmental changes (Ali, et al., 2018). Similarly, the *ahyR* gene encodes a receptor protein that responds to these QS signals, regulating the expression of various virulence-associated genes (Bi, et al., 2007). The *ahyR* has been shown to be pivotal in modulating *A. hydrophila*'s response to environmental cues, thereby enhancing its infection capabilities (Fernando and Judan Cruz, 2020). Furthermore, the presence of *csgA* may contribute to the structural integrity of the biofilm matrix, aiding in bacterial adhesion and persistence in diverse environments (Yan, et al., 2020). This gene is pivotal in curli fimbriae production, which are essential for cell-to-cell interactions and surface attachment, forming the backbone of the biofilm structure (Dueholm, et al., 2011). These genes collectively enhance the biofilm-forming abilities and pathogenic potential of *A. hydrophila*, making them critical targets for understanding and managing infections caused by this bacterium.

This study embarks on an investigation into the biofilm-forming capabilities of four *A. hydrophila* strains, sourced from the American Type Culture Collection (ATCC) and the Korean Collection for Type Cultures (KCTC), on materials routinely used as food contact surfaces. The chosen materials—stainless steel (SS), silicon rubber (SR), polyethylene terephthalate (PET), and high-density polyethylene (HDPE)—are ubiquitous in food processing and packaging owing to their functional properties (Ashrafudoulla, et al., 2023). Understanding biofilm formation and detachment on these surfaces is crucial for developing effective sanitation protocols and biofilm control measures. Moreover, this study evaluates the antibiotic sensitivity, motility, and gene expression profiles of the *A. hydrophila* strains to gain a holistic understanding of their adaptive mechanisms and potential resistance to control measures for bacterial contamination in the food industry.. Furthermore, molecular insights into biofilm development and resistance were obtained through reverse transcription PCR (RT-PCR) and visualization techniques such as confocal laser scanning microscopy (CLSM) and scanning electron microscopy (SEM) were incorporated. By integrating these multidisciplinary approaches, this research aims to deepen the understanding of *A. hydrophila* biofilms and their implications for food safety. The findings are expected to inform the development of more effective biofilm control strategies, ultimately contributing to safer food processing and packaging practices.

Materials and methods

Bacterial strain, culture media, and growth conditions

This study employed four strains of *A. hydrophila* sourced from the ATCC and KCTC. The strains used were ATCC 15467, ATCC 7966, KCTC 2356, and KCTC 11533. Each strain, stored at -80°C in 40 % glycerol, was revived by inoculating 100 μL of the bacterial stock into a 50 mL conical tube (SPL Life Sciences, Gyeonggi-do, Republic of Korea) containing 10 mL of LB broth (Becton, Dickinson, and Company [BD], Sparks, MD, USA). The cultures were then grown in a shaking incubator (VS-8480SF, Vision Scientific, Gyeonggi-do, Republic of Korea) at 30°C and 220 rpm for 24 h. The bacteria were subsequently cultured at 30°C for another 24 h. Following incubation, the cultures were centrifuged at 10,000 rpm, 4°C , for 10 min. The resulting bacterial pellet was washed

twice with 10 mL of phosphate-buffered saline (PBS; Oxoid, Basingstoke, UK). The initial bacterial concentration was determined using the plate count method on LB agar (Sigma-Aldrich Chemie, GmbH, Germany) and was found to be between 10^8 and 10^9 log CFU/mL. For further experiments, the bacteria were diluted using 0.1 % peptone water (PW; Oxoid) due to its ability to provide a nutrient-rich environment that helps maintain bacterial viability during the experimental procedures. However, it can also prevent cellular stress and maintain metabolic activity over longer periods, which is particularly important in ensuring consistent and reliable results.

Preparation of surfaces (SS, SR, PET, HDPE)

Four materials, including SS ($2 \times 2 \text{ cm}^2$; thickness: 0.1 cm; Chung-Ang Scientific, Inc., Seoul, Korea), SR ($2 \times 2 \text{ cm}^2$; thickness: 0.2 cm; Komax Industrial Co., Ltd., Seoul, Korea), plastic (PET; $2 \times 2 \text{ cm}^2$; thickness: 0.27 mm; Chung-Ang Scientific, Inc.), and HDPE ($2 \times 2 \text{ cm}^2$; thickness: 0.6 cm; Green Industrial Co., Gyeongsangnam, Republic of Korea), were selected for the experiment due to their common use as food contact surfaces in the food industry. According to methods adapted from previous research (Ashrafudoulla, et al., 2024a), the SS, SR, and HDPE coupons, placed in a sealed beaker, were sterilized in an autoclave and then dried in a dry oven for 48 h. Differently, PET coupons were first submerged in 100 % methanol (Daejung Che. & Metals Co. Ltd., Korea) for 1 h at room temperature, followed by submersion in 70 % ethanol (Daejung Che. & Metals Co. Ltd., Korea) (for 1 h at 25°C) before washing three more times. Each side of the coupons was then exposed to UV light at $1,000 \text{ W/cm}^2$ for 15 min to ensure the removal of remaining flora.

Biofilm formation

A strategy for analyzing biofilm development and detachment was adapted from a previously established method (Jahid, et al., 2013). Food contact surfaces were prepared as described in the section 2.2. Each coupon (SS, SR, PET, and HDPE) was placed in a 50 mL Falcon tube containing 10 mL of LB broth, serving as the biofilm test culture medium. Before the experiment, each strain of *A. hydrophila* (ATCC 15467, ATCC 7966, KCTC 2356, and KCTC 11533) was standardized to a concentration of 10^6 log CFU/mL to ensure a consistent initial bacterial load for the biofilm formation tests, mimicking realistic microbial conditions for biofilm development on submerged surfaces. Biofilm formation was monitored over 24, 48, 72 h, and 96 h with the media being refreshed every 24 h. To remove the biofilm from the surfaces, the coupons were placed in a tube containing 10 mL of PW and 10 sterile beads, then vortexed for 1 min. The resulting solutions were serially diluted and spread onto LB agar plates to quantify the remaining bacterial cells.

Antibiotic sensitivity test

Four strains of *A. hydrophila* (ATCC 15467, ATCC 7966, KCTC 2356, and KCTC 11533) were tested for their antibiotic sensitivities using the disk diffusion method on Mueller-Hinton agar (Oxoid) in this study. Cultures of each strain were grown on LB agar and broth until they reached the logarithmic phase. These cultures were then standardized to a 0.5 McFarland turbidity standard to ensure consistent inoculum density. The standardized suspensions were evenly spread on the Mueller-Hinton agar plates, onto which antibiotic-impregnated disks were placed. After incubating at 30°C for 24 h, the zones of inhibition around the disks were measured and compared to clinical breakpoints to determine whether each strain was sensitive, intermediately susceptible, or resistant to the antibiotics tested (CLSI, 2016). The multiple antibiotic resistance index (MARI) was calculated using a specific formula (Krumperman, 1983):

$$\text{MARI} = \frac{\text{number of antibiotics to which the isolate is resistant}}{\text{total number of antibiotics to which the isolate has been exposed}}$$

Swimming and swarming motility

The movement of bacteria in aqueous media via flagella is termed “swimming,” whereas “swarming” refers to movement on a solid surface using lateral flagella, characterized by a rapid, collective movement (Wadhwa and Berg, 2022). Both motility assays were performed based on (Jahid, Lee, Kim and Ha, 2013) with modifications. To assess the swimming motility of *A. hydrophila*, 2 μL of bacterial cell suspension was placed in the center of an agar-nutrient plate containing 0.3 % Bacto-Agar (Difco, BD), followed by incubation at 30 °C for 12 h. Swarming motility was evaluated by incubating an equal number of bacteria on an agar-nutrient plate with 0.5 % Bacto-Agar for 12 h at 30 °C. The motility diameter on the plate was then measured in millimeters.

Gel electrophoresis

Gel electrophoresis was conducted to confirm the effectiveness of the newly designed primers used in this investigation. DNA from four strains of *A. hydrophila* (ATCC 15467, ATCC 7966, KCTC 2356, and KCTC 11533) was isolated using the DNeasy Blood & Tissue Kit (Qiagen, Hilden, Germany). The primer pairs, designed using NCBI-BLAST and detailed in Table 1, were synthesized by Bioneer Corp. (Daejeon, Korea). PCR reactions were performed using a Bio-Rad T100 Thermal Cycler under the following conditions: initial denaturation at 95 °C for 2 min, followed by 34 cycles of denaturation at 95 °C for 30 s, annealing at 55 °C for 1 min, and extension at 72 °C for 30 s. This was followed by a final extension at 72 °C for 5 min and a hold at 4 °C. Subsequently, 2 % agarose gel electrophoresis was conducted at 100 V for 20 min. The gel was then visualized using the Molecular Imager® Gel Doc™ XR System.

RT-PCR

Biofilm cell aggregates from four strains of *A. hydrophila* on different surfaces were prepared for RT-PCR analysis. The procedure began with culturing the strains for 48 h to induce biofilm formation on four different surfaces. Post-incubation, the biofilm cells were detached using previously established protocols (Ashrafudoulla, Park, Toushik, Shaila, Ha, Rahman, Park and Ha, 2024a). The detached cells were then centrifuged to pellet the bacterial cells, followed by careful removal of the supernatant. The cell pellets were rinsed twice with PBS to remove any non-adherent cells and residual media. Following this, total RNA was extracted from the bacterial cell aggregates. These RNA samples, representing the biofilm-associated cells, were designated as the treatment group, while RNA extracted from planktonic bacterial cells served as the control. The RNeasy Mini Kit from Qiagen was used according to the manufacturer’s instructions. This kit enabled the efficient extraction of high-quality RNA, which was essential for precise subsequent molecular analysis. After extracting RNA, cDNA was synthesized using the Maxime RT PreMix Kit (iNtRON Biotechnology Gyeonggi, Republic of

Korea) following the kit instructions. The RT-PCR process transforms the harvested RNA into cDNA in preparation for gene expression analysis.

The 7500 Fast Real-Time PCR System (Applied Biosystems, Alameda, CA, USA) was used to measure relative gene expression levels. Each PCR reaction contained 10 μL of SYBR Green PCR Master Mix (Applied Biosystems), 0.8 μL of forward and reverse primers (10 pmol each), 2 μL of synthesized cDNA, and 7.2 μL of distilled water, making a total volume of 20 μL . This composition guarantees the ideal conditions for enhancing specific gene sequences and precisely evaluating their expression levels in the examined *A. hydrophila* strains. The $2^{-\Delta\Delta\text{Ct}}$ method (Livak and Schmittgen, 2001) was used to calculate the relative gene expression. This method allows for the normalization of target gene expression to a reference (housekeeping) gene and comparison between biofilm-associated cells (treatment group) and planktonic bacterial cells (control group).

CLSM

The experiment was conducted following several established research methods (Ashrafudoulla, Park, Toushik, Shaila, Ha, Rahman, Park and Ha, 2024a). Initially, 400 μL of each *A. hydrophila* strain, diluted to a concentration of 10^6 CFU/mL, was inoculated onto a confocal dish (SPL Life Sciences) to form biofilms. The dishes were incubated at 37 °C for 24 h. Subsequently, the dishes were carefully washed three times with PBS to remove any residues. The cells were then stained with Film Tracer™ Live/Dead biofilm viability kit contain SYTO-9 and propidium iodide (PI) (Invitrogen life technologies, 29851 Willow Creek Rd Eugene, OR 97402) and observed using a confocal laser scanning microscope (Carl Zeiss, Oberkochen, Germany). A 488 nm argon laser set at 0.2 % intensity with a 40X underwater objective was used. SYTO-9 (green) emission fluorescence was measured between 410 and 605 nm, while PI (red) emission fluorescence was measured between 645 and 700 nm.

SEM

FE-SEM analysis was conducted to examine the 48-h-old biofilm on PET surfaces of the four selected strains (Section 2.1) using the methods of (Ashrafudoulla, et al., 2024b). The specimens were first fixed using 2.5 % glutaraldehyde solution (Sigma-Aldrich Chemie, GmbH, Germany), sequentially dehydrated with an ethanol series, then coated with platinum, and finally visualized using an FE-SEM instrument (ultra-high-resolution FE-SEM-SU8600; Hitachi, Tokyo, Japan).

Statistical analysis

Each experiment was conducted in triplicate. The data are represented using the mean value with standard deviation (\pm SD) as a measure of central tendency. Data analysis was performed using Microsoft 365 and GraphPad Prism software (Version 9.0; GraphPad Software, Inc., La Jolla, CA, USA).

Table 1

Primer details for gene analysis used in the present study.

Gene	Base sequence (5'→3')	Amplicon size (bp)	T_m (°C)	GC%	Self-Complementary	3'-Self Complementary	
16S	F	GGCAGTCTCCCTTGAGTTC	153	60.04	60.00	5.00	0.00
	R	CAGAGATGTGGGAGTGCCTT		59.38	55.00	3.00	0.00
luxS	F	CCATGCAGACCCCGAACA	121	60.30	57.89	4.00	0.00
	R	ATGAAGCCGGCAAACAGATG		59.19	50.00	6.00	2.00
ahyR	F	GAGCGAACCGTGAAC TACCA	72	60.04	55.00	4.00	0.00
	R	GATGGCCTGGTAGCGATTCA		59.89	55.00	4.00	1.00
csgA	F	CCCGTCTGCTATTTC CGGTT	325	60.04	55.00	2.00	0.00
	R	GGTAGCTGTATCGACTGCC		59.97	60.00	4.00	0.00

F, forward; R, reverse.

Table 2Biofilm formation (log CFU/cm²) of various *Aeromonas hydrophila* strains on different surface materials (SS, SR, PET, and HDPE) across incubation periods (24-96).

Strain	Hours	SS (log CFU/cm ²)	SR (log CFU/cm ²)	PET (log CFU/cm ²)	HDPE (log CFU/cm ²)
ATCC 15467	24	4.05 ± 0.47**	4.66 ± 0.44**	4.57 ± 0.31**	4.58 ± 0.37**
	48	5.93 ± 0.07	5.83 ± 0.05	5.73 ± 0.58	5.92 ± 0.08
	72	6.20 ± 0.03*	6.14 ± 0.12*	6.24 ± 0.07*	6.04 ± 0.06
	96	4.03 ± 0.06**	4.22 ± 0.10**	4.28 ± 0.15**	4.06 ± 0.17**
ATCC 7966	24	3.83 ± 0.39**	4.29 ± 0.72**	3.92 ± 0.30**	4.15 ± 0.51**
	48	5.81 ± 0.10	5.82 ± 0.09	6.00 ± 0.11*	5.78 ± 0.06
	72	6.27 ± 0.06*	6.28 ± 0.12*	6.50 ± 0.08*	6.01 ± 0.10
	96	4.29 ± 0.06**	5.03 ± 0.06	4.94 ± 0.14**	4.45 ± 0.20**
KCTC 2358	24	4.19 ± 0.07**	4.96 ± 0.73	5.07 ± 0.13	5.01 ± 0.09
	48	5.48 ± 0.08	5.91 ± 0.06*	5.58 ± 0.33	5.21 ± 0.10
	72	5.92 ± 0.12	6.15 ± 0.12*	6.09 ± 0.11*	5.81 ± 0.38
	96	4.27 ± 0.06**	4.88 ± 0.27	4.85 ± 0.08**	4.72 ± 0.23**
KCTC 11533	24	4.20 ± 0.09**	4.97 ± 0.14	4.78 ± 0.10	4.70 ± 0.12
	48	5.33 ± 0.10	5.40 ± 0.10	5.61 ± 0.06*	5.25 ± 0.06
	72	6.02 ± 0.09*	5.47 ± 0.12	5.98 ± 0.27**	5.69 ± 0.22
	96	4.18 ± 0.09**	4.78 ± 0.07	4.64 ± 0.07**	4.15 ± 0.05**

Statistical Analysis Using Pairwise t-tests was done.

* indicates that the biofilm formation is significantly different ($P < 0.05$) when compared to other surfaces or time points within the same strain.** indicates that the biofilm formation is significantly lower ($P < 0.05$) compared to the highest observed value for the same strain across all surfaces. SS, stainless steel; SR, silicon rubber; PET, polyethylene; HDPE, high-density polyethylene.

Results and Discussions

Biofilm formation

The biofilm formation potential of four *A. hydrophila* strains—ATCC 15467, ATCC 7966, KCTC 2358, and KCTC 11533—was systematically evaluated on stainless steel (SS), silicon rubber (SR), polyethylene terephthalate (PET), and high-density polyethylene (HDPE) surfaces over incubation periods of 24, 48, 72, and 96 h. Across all strains and surfaces, biofilm formation peaked at 72 h, followed by a significant decline at 96 h, indicative of biofilm degradation or detachment. ATCC 15467 exhibited consistently high biofilm formation across surfaces, with peak levels at 72 h on PET (6.24 ± 0.07 log CFU/cm², $P < 0.05$) and SR (6.14 ± 0.12 log CFU/cm², $P < 0.05$). SS also supported significant biofilm development (6.20 ± 0.03 log CFU/cm², $P < 0.05$), while HDPE demonstrated comparatively lower levels (6.04 ± 0.06 log CFU/cm²). By 96 h, biofilm stability diminished markedly across all surfaces, reflecting the dynamic nature of biofilm development. ATCC 7966 emerged as the most prolific biofilm producer, achieving the highest biofilm density observed in the study at 72 h on PET (6.50 ± 0.08 log CFU/cm², $P < 0.05$). Comparable levels were recorded on SR (6.28 ± 0.12 log CFU/cm², $P < 0.05$) and SS (6.27 ± 0.06 log CFU/cm², $P < 0.05$). Notably, biofilm formation on HDPE was less pronounced (6.01 ± 0.10 log CFU/cm²), and at 96 h, all surfaces exhibited a significant reduction in biofilm density, particularly on HDPE (4.45 ± 0.20 log CFU/cm²).

KCTC 2358 demonstrated a surface preference for SR and PET, reaching peak biofilm formation at 72 h (6.15 ± 0.12 log CFU/cm² and 6.09 ± 0.11 log CFU/cm², respectively, $P < 0.05$). SS supported moderate biofilm formation (5.92 ± 0.12 log CFU/cm²), while HDPE exhibited the lowest biofilm levels (5.81 ± 0.38 log CFU/cm²). The decline in biofilm formation at 96 h was most pronounced on HDPE and PET surfaces. KCTC 11533 exhibited notable biofilm formation on SS at 72 h (6.02 ± 0.09 log CFU/cm², $P < 0.05$), followed by moderate levels on PET (5.98 ± 0.27 log CFU/cm²) and SR (5.47 ± 0.12 log CFU/cm²). HDPE supported the lowest biofilm levels (5.69 ± 0.22 log CFU/cm² at 72 h). By 96 h, significant reductions were evident across all surfaces, underscoring the time-dependent nature of biofilm stability (Table 2).

Surface-specific trends reveal PET and SR as the most conducive substrates for biofilm development, likely due to their hydrophobicity and microstructural properties. In contrast, HDPE consistently demonstrated the lowest biofilm formation, suggesting its potential as a biofilm-resistant material in industrial applications. Our study observed significant diversity in biofilm formation among bacterial strains,

echoing the results of previous research. For instance, Sehree, et al. highlighted that the ability of bacterial strains to form biofilms can differ considerably, a phenomenon attributed to their unique genetic and phenotypic traits (Sehree, et al., 2022). A salient feature of our study was that the strain ATCC 7966 demonstrated the highest biofilm formation among the four strains examined herein. Consistent with our findings, Elhariry reported that ATCC 7966 exhibited the highest biofilm formation among *A. hydrophila* strains (Elhariry, 2011). Similarly, Jahid et al. documented an average biofilm density of 5.4 log CFU/cm² for *A. hydrophila*, highlighting the notable biofilm-forming ability of specific strains (Jahid, et al., 2018).

In addition to the bacterial strain, the surface type significantly influences biofilm formation, as evidenced by the relatively higher biofilm levels on PET and SR surfaces. The literature indicates that synthetic polymers like PET and SR often support robust biofilm formation due to their surface properties and hydrophobic nature (Rather, et al., 2021). Hydrophobic surfaces provide a stable environment for microbial attachment (Donlan, 2002). According to (Al-Amshawee, et al., 2021), surface characteristics like roughness and wettability are key determinants of bacterial adhesion. However, Lackner et al. noted that the literature does not consistently define the optimal wettability range for efficient microbial adhesion, suggesting that multiple factors come into play (Lackner, et al., 2009). These factors include the composition of EPS, nutrient availability, and the sequence of microbial colonization. In addition to the hydrophobicity of SR, its elastomeric nature results in a rougher surface, offering more sites for microbial adherence (Mitik-Dineva, et al., 2009). PET, although smoother, can adsorb organic compounds, creating nutrient-rich conditions conducive to biofilm growth (Lejeune, 2003). Furthermore, SR can leach low molecular weight compounds that nourish microorganisms, enhancing biofilm development (Busscher, et al., 1995). In contrast, SS, especially when polished, has a smooth, high-energy surface that interacts more with water, making microbial adherence more challenging (Zottola and Sasahara, 1994). HDPE, while hydrophobic, tends to be smoother and more inert than SR and PET, reducing microbial attachment points (Lejeune, 2003). Environmental exposure to moisture and organic matter also plays a role, as these conditions are more common in settings where SR and PET are used, further promoting biofilm formation (Vickery, et al., 2004).

Our results demonstrated that incubation time played a critical role in biofilm formation, with biofilm levels reaching their peak at 72 h across all surfaces. This stage reflects the mature phase of biofilm development, characterized by high cell density and robust structural organization. However, at 96 h, a significant reduction in biofilm levels

was observed, suggesting biofilm degradation or detachment. This decline indicates that the biofilm had progressed to its final developmental stage, where cell death and dispersal occur, enabling the release of biofilm cells to colonize new surfaces. Such behavior aligns with the natural biofilm life cycle, where aging biofilms undergo cellular turnover and release planktonic cells, facilitating the establishment of new biofilm communities. This dynamic process underscores the balance between biofilm stability and renewal, driven by environmental and biological factors. This observation aligns with the standard biofilm development cycle outlined in the relevant literature. In particular, Elhariry recorded *A. hydrophila* biofilms ranging from 2.85 to 3.95 log CFU/cm² at 24 h, a finding that mirrors the results of our study (Elhariry, 2011).

Antibiotic resistance test

The antibiotic susceptibility testing of four *A. hydrophila* strains—ATCC 15467, ATCC 7966, KCTC 2358, and KCTC 11533—unveiled unique resistance patterns across a spectrum of 20 antibiotics, as evidenced by their MAR indices (Table 3). Except for ATCC 7966 and KCTC 2358, which exhibited a MARI of 0.65, the other strains demonstrated a higher level of resistance, with a MARI of 0.80. The antibiotic resistance patterns revealed significant variability among the tested strains. ATCC 15467 demonstrated resistance to 16 antibiotics, including critical agents such as ampicillin, cefotaxime, and meropenem, while showing susceptibility to amikacin, doxycycline, minocycline, and nalidixic acid. In contrast, ATCC 7966 exhibited resistance to 13 antibiotics, including ampicillin and clindamycin, but remained susceptible to amikacin, chloramphenicol, cefotaxime, and doxycycline. Similarly, KCTC 2358 displayed resistance to 13 antibiotics, particularly against ampicillin, cefepime, and meropenem, while retaining susceptibility to amikacin, chloramphenicol, and doxycycline. KCTC 11533 demonstrated resistance to 16 antibiotics, including

Table 3
Antimicrobial susceptibility profiles and MARI of four *Aeromonas* strains against 20 antibiotics.

Sl. No.	Name of Antibiotics	Antibiotic Contents per disc (µg)	ATCC 15467	ATCC 7966	KCTC 2358	KCTC 11533
1	Amikacin (AN)	30	R	S	S	R
2	Ampicillin (AM)	10	R	R	R	R
3	Cefepime (FEP)	30	S	I	R	I
4	Cefotaxime (CTX)	30	R	I	R	R
5	Ceftazidime (CAZ)	30	I	I	R	R
6	Ceftriaxone (CRO)	30	I	I	R	R
7	Chloramphenicol (C)	30	I	S	S	S
8	Ciprofloxacin (CIP)	5	I	S	S	I
9	Clindamycin (CC)	2	R	R	R	R
10	Doxycycline (D)	30	S	S	S	S
11	Erythromycin (E)	15	R	R	R	R
12	Gentamicin (GM)	10	R	S	S	R
13	Imipenem (IPM)	10	I	R	I	R
14	Kanamycin (K)	30	I	S	I	R
15	Levofloxacin (LVX)	5	I	I	S	S
16	Meropenem (MEM)	10	R	R	R	R
17	Minocycline (MI)	30	S	I	I	S
18	Nalidixic acid (NA)	30	S	S	I	R
19	Penicillin (P)	10	R	R	R	R
20	Tetracycline (TTX)	30	I	I	S	I
	MARI		0.80	0.65	0.65	0.80

clindamycin, tetracycline, and cefotaxime, while retaining susceptibility to chloramphenicol, doxycycline, and levofloxacin.

The present study underscores the critical issue of multidrug resistance in *A. hydrophila*. Our findings of high-level resistance to beta-lactams, carbapenems, lincosamides, and tetracyclines are consistent with the established intrinsic resistance profile of this genus (Martins, et al., 2023). The co-occurrence of multiple resistance mechanisms, including chromosomally encoded beta-lactamases, metallo-beta-lactamases, methyltransferases, efflux pumps, and ribosomal protection proteins, as previously reported (Bahr, et al., 2021; Hernould, et al., 2008; Ma, et al., 2023; ROSSOLINI, et al., 1996), likely contributes significantly to this broad-spectrum resistance phenotype.

Motility

The swimming and swarming motility of four *A. hydrophila* strains were assessed. Strain ATCC 15467 exhibited relatively low swimming motility, averaging 10.0 ± 2.0 mm, and minimal swarming motility, consistently measuring 2.0 ± 0.0 mm. Strain ATCC 7966 showed moderate motility, with average swimming and swarming motilities of 39.0 ± 3.6 and 21.7 ± 3.2 mm, respectively. The KCTC 2358 strain demonstrated relatively higher motility, with an average swimming motility of 55.3 ± 4.9 mm and an average swarming motility of 47.7 ± 3.5 mm. Finally, KCTC 11533 exhibited the highest motility among the strains tested, with average swimming and swarming motilities of 76.0 ± 6.6 and 31.0 ± 3.6 mm, respectively. These results highlight significant strain-specific differences in both swimming and swarming capabilities, with KCTC 11533 and 2358 being the most motile. In the qualitative observations, ATCC 15467 showed a featureless mat in both assays, consistent with its low motility scores. ATCC 7966 formed a featureless mat in the swimming assay but exhibited a small, centralized colony in the swarming assay, indicating limited swarming capability. In contrast, KCTC 2358 formed a distinct "bull's eye" pattern in both assays, reflecting its strong motility. Similarly, KCTC 11533 displayed a vortex-like pattern, particularly prominent in the swarming assay, indicating robust motility (Fig. 1).

The observed variations in swimming and swarming motility among the four *A. hydrophila* strains underscore the phenotypic diversity within this species. These motility patterns are similar to those published by (Kearns, 2010). Motility is a critical virulence factor, enabling bacteria to colonize different host niches, invade tissues, and evade the immune system (Janda and Abbott Sharon, 2010). The significantly higher motility exhibited by KCTC 2358 and 11533 suggests a potentially enhanced ability to colonize and disseminate within a host compared to the other strains.

The distinct colony morphologies observed in the swarming assay correlate with the quantitative motility data. The "bull's eye" pattern displayed by KCTC 2358 is characteristic of highly motile bacteria and is often associated with the production of surface-active compounds (O'Toole and Kolter, 1998). The vortex-like pattern exhibited by KCTC 11533 suggests a complex interplay of flagellar-mediated movement and hydrodynamic forces, possibly contributing to its exceptional swarming ability.

Gel electrophoresis

The gel electrophoresis profile clearly demonstrated the presence and distribution of specific genes across four bacterial strains: ATCC 15467, ATCC 7966, KCTC 2358, and KCTC 11533 (Fig. 2). The amplification of the 16S *rRNA* gene (PCR product band at 153 bp) across all strains confirmed DNA's successful extraction and amplification, serving as a reliable positive control. The *luxS* gene (PCR product band at 121 bp) was present in all four strains, indicating its conserved role in QS among these bacteria. Similarly, the *ahyR* gene, detected at 72 bp, was consistently found in all strains, further underscoring its involvement in regulatory processes common to these species. Interestingly, the *csaG*

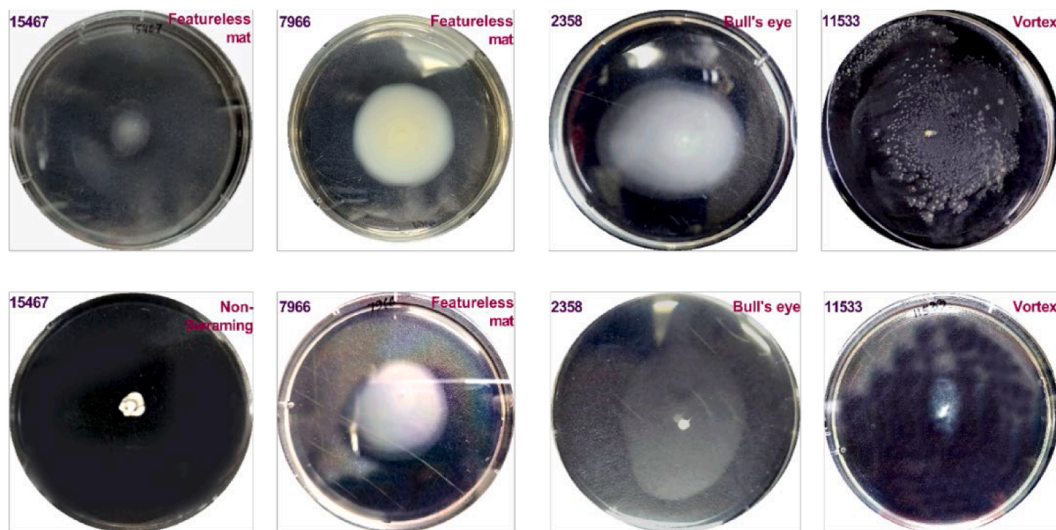
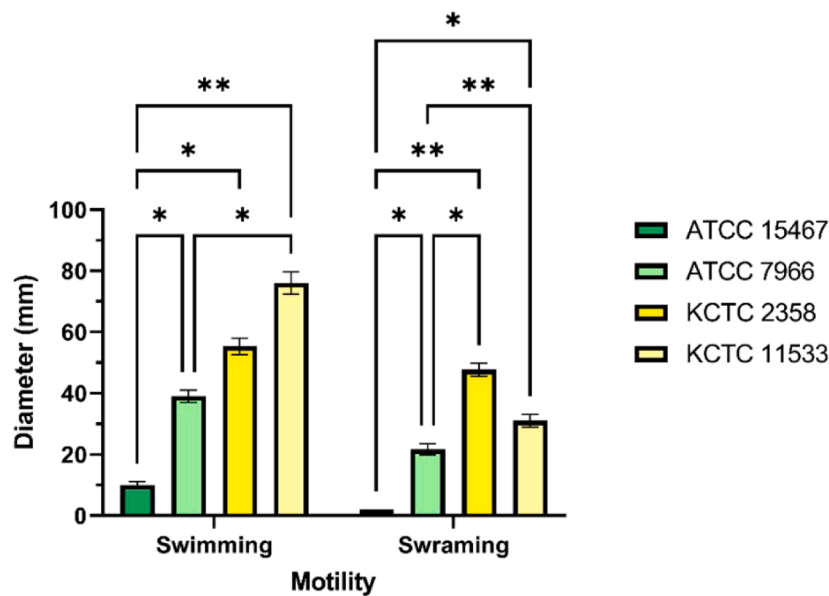


Fig. 1. Comparative analysis of swimming and swarming motility among *A. hydrophila* strains (ATCC 15467, ATCC 7966, KCTC 2358, KCTC 11533) using two-way ANOVA followed by tukey's multiple comparison, represented by motility diameters (mm). Asterisks indicate significance levels: * $P < 0.05$, ** $P < 0.01$.

gene, expected at 325 bp, was only present in ATCC 7966, not in ATCC 15467, KCTC 2358, and KCTC 11533, thus highlighting a potential divergence in the genetic makeup and functional capabilities of these bacteria. It may be that *csgA* plays a unique role in ATCC 7966, possibly related to biofilm formation or other structural functions not shared by the other strains. These results highlight the variations in the distribution of QS and biofilm-related genes across different bacterial strains, providing insights into their potential roles in microbial behavior and adaptation.

The successful amplification of the universal bacterial marker, the 16S rRNA gene, in all strains, serves as a robust positive control, validating the quality of DNA extraction and PCR amplification (Gutell, et al., 1994). The consistent presence of the *luxS* gene across all strains strongly implies its conserved role in QS within this bacterial group (Ali, Yao, Li, Sun, Lin and Lin, 2018), as it suggests the potential for cell-to-cell communication, a critical factor in biofilm development (Wang, et al., 2019). Similarly, the detection of the *ahyR* gene in all

strains points to its conserved involvement in regulatory functions and its role in the regulation of virulence (Bi, Liu and Lu, 2007). This gene is likely integral to maintaining cellular homeostasis and responding to environmental cues.

The most intriguing finding was the exclusive presence of the *csgA* gene in the ATCC 7966 strain. This strain-specific occurrence suggests a unique adaptive strategy employed by ATCC 7966. Given the association of *csgA* with biofilm formation in many bacteria, mainly in *Escherichia coli* (Lv, et al., 2020), it is plausible that this strain exhibits enhanced biofilm-forming capabilities compared to the other strains. This could provide ATCC 7966 with a competitive advantage in certain environments by facilitating colonization and protection from external stressors. The absence of *csgA* in the remaining strains highlights potential differences in their ecological niches and lifestyles. These strains may rely on alternative mechanisms for surface attachment and community formation.

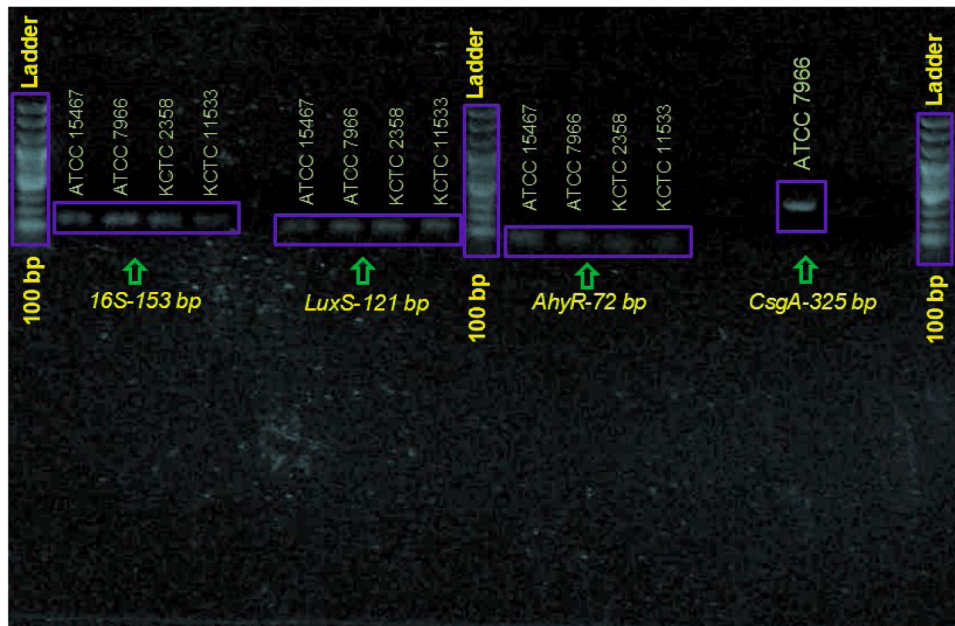


Fig. 2. PCR amplification results of four *A. hydrophila* strains (ATCC 15467, ATCC 7966, KCTC 2358, KCTC 11533) for the detection of four genes: *16S* (153 bp), *luxS* (121 bp), *ahvR* (72 bp), and *csgA* (325 bp). The 100 bp ladder was used in this experiment.

Gene expression

In this study, we investigated the effects of various surface materials (SS, SR, PET, and HDPE) on the expression of the *luxS*, *ahvR*, and *csgA* genes across four bacterial strains (ATCC 15467, ATCC 7966, KCTC 2358, and KCTC 11533). Biofilm cells of ATCC 15467 on SS, SR, and HDPE surfaces showed significant downregulation of *luxS*, with moderate suppression observed when the biofilm was grown on PET. In contrast, *ahvR* showed slight upregulation (SS surface), moderate downregulation (SR and HDPE surfaces), or significant upregulation (PET surface). These results suggest that gene expression in biofilm cells is substantially influenced by the surface material, with biofilm on PET showing enhanced *ahvR* activity, whereas biofilm on SS and HDPE surfaces generally displays suppressed *luxS* (Fig. 3).

In biofilm cells of ATCC 7966, *luxS* remained relatively stable irrespective of the surface, with only slight downregulation (SS and SR surfaces) or minor variations (PET and HDPE surfaces) observed. Biofilm formed on SS and SR showed moderate downregulation of the *ahvR* gene, whereas this same gene was moderately and significantly upregulated in biofilm cells grown on HDPE and PET, respectively, indicating heightened QS activity on PET. The *csgA* gene was largely suppressed when biofilm was formed on SS, SR, and PET surfaces, with minimal expression detected in the biofilm cells grown on HDPE, suggesting that the surface material significantly affects *csgA* expression; the differential expression of *ahvR* and *csgA* in biofilm on PET surface as a case in point.

For KCTC 2358, the surface material profoundly affected the regulation of QS genes. The *luxS* gene was strongly upregulated when biofilm was formed on SS, suggesting that SS promotes QS activities that could enhance biofilm formation and pathogenicity. In contrast, SR, PET, and HDPE surfaces led to the downregulation of *luxS*, indicating a suppressive effect on QS. The *ahvR* gene mirrored this trend; its highest expression occurred in biofilm formed on SS surface, whereas it was moderately upregulated in biofilm formed on SR, PET, and HDPE surfaces, highlighting the potential of SS to enhance QS, while other surfaces might inhibit these activities.

In KCTC 11533, *luxS* expression was strongly upregulated in the biofilm cells formed on SS and SR surfaces, potentially enhancing QS and biofilm formation. In comparison, PET and HDPE surfaces resulted

in more moderate upregulation of *luxS*. The *ahvR* gene showed mild upregulation irrespective of the surface on which the biofilm was grown, with SS surface having the most pronounced effect. These findings suggest that SS and SR surfaces have the most substantial impact on *luxS* expression, while *ahvR* remains relatively consistent across different materials.

The surface material strongly influences bacterial gene expression. SS often stimulates QS (Chen, et al., 2020; Dula, et al., 2021; Zanzan, et al., 2024), whereas PET shows mixed effects. SR and HDPE generally suppress gene activity (Gu and Ren, 2014). These findings suggest that surface properties play a crucial role in biofilm formation and bacterial behavior. Further research is needed to understand the underlying mechanisms.

Overall, the analysis indicates that the surface material plays a critical role in modulating the expression of QS and biofilm-related genes across these bacterial strains. SS and PET surfaces, in particular, demonstrate significant potential to influence these regulatory mechanisms, highlighting their importance in bacterial biofilm dynamics and pathogenicity.

CLSM

The CLSM images provided a comprehensive analysis of the structural and functional dynamics of four bacterial strains—ATCC 15467, ATCC 7966, KCTC 2358, and KCTC 11533—over four time frames: 24, 48, 72, and 96 h. For ATCC 15467, at 24 h (Fig. 4A), scattered cells with low fluorescence intensity suggest the initial colonization phase. By 48 h (Fig. 4B), increased cell density and fluorescence indicate active biofilm growth. At 72 h (Fig. 4C), a dense biofilm structure with high green fluorescence reflects the mature biofilm phase, signifying peak biofilm development. By 96 h (Fig. 4D), the presence of red fluorescence marks biofilm aging and cell death, suggesting a shift from growth to biofilm degradation and detachment, a process that potentially promotes the formation of new biofilm colonies. For ATCC 7966, early biofilm formation is evident at 24 h (Fig. 4E), with moderate fluorescence reflecting the early adhesion phase. By 48 h (Fig. 4F), dense clustering and higher fluorescence indicate rapid biofilm development. At 72 h (Fig. 4G), the biofilm appears fully developed with strong green fluorescence, corresponding to its maturation phase. By 96 h (Fig. 4H),

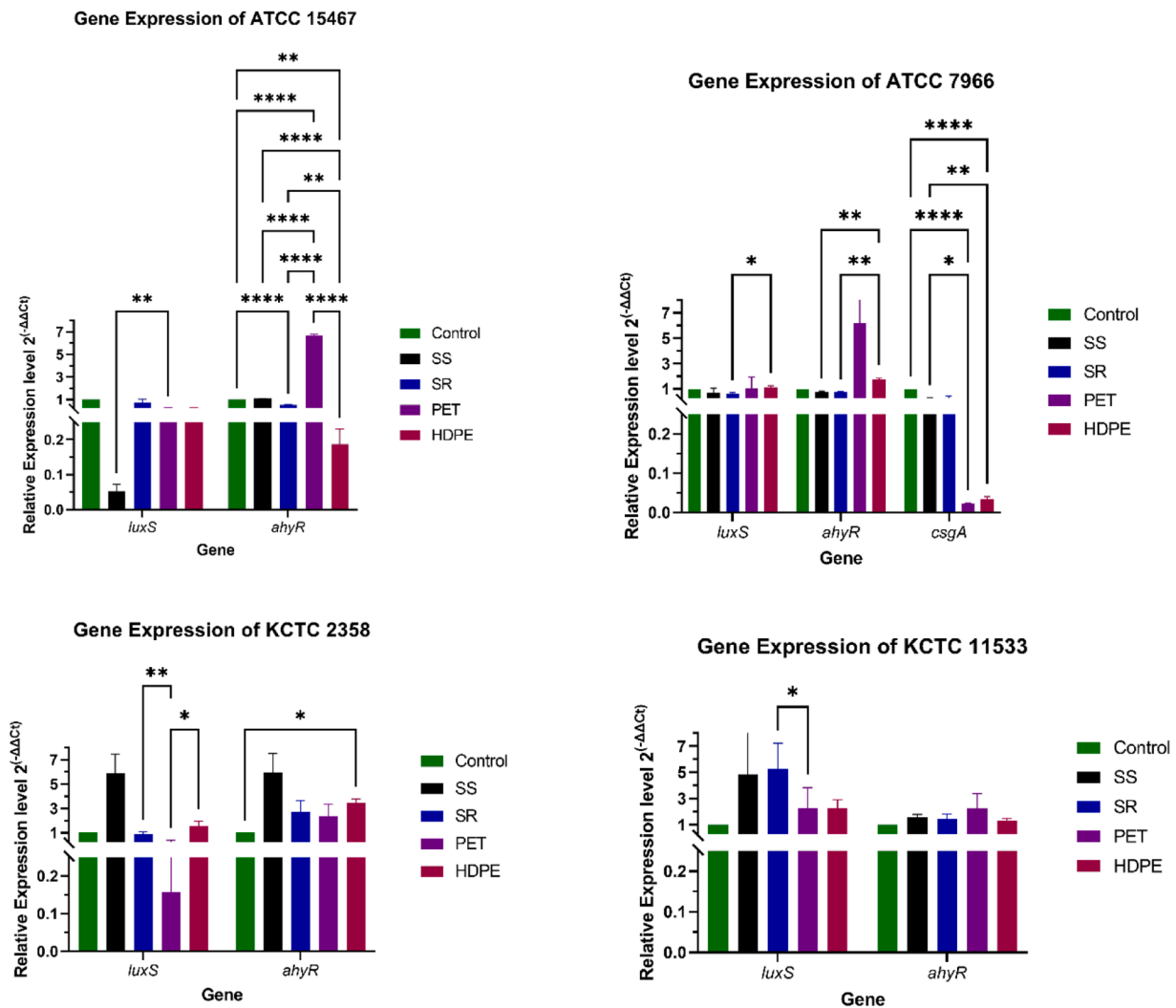


Fig. 3. Relative gene expression of *luxS*, *ahvR*, and *csgA* in biofilms of *A. hydrophila* strains (ATCC 15467, ATCC 7966, KCTC 2358, KCTC 11533) formed on various food contact surfaces (SS, SR, PET, HDPE) compared to control conditions, analyzed using two-way ANOVA followed by tukey's multiple comparison to determine significant differences. Asterisks indicate significance levels: * $P < 0.05$, ** $P < 0.01$, *** $P < 0.001$, **** $P < 0.0001$.

widespread red fluorescence signifies the final stage of biofilm development, with substantial cell death and detachment, facilitating potential release of planktonic cells for new biofilm initiation.

For KCTC 2358, at 24 h (Fig. 4I), sparse cell adhesion and low fluorescence are observed, indicative of the initial attachment stage. By 48 h (Fig. 4J), increased clustering and moderate fluorescence reflect active biofilm formation and growth. At 72 h (Fig. 4K), a dense and mature biofilm structure emerges with strong fluorescence, representing the peak development phase. By 96 h (Fig. 4L), prominent red fluorescence indicates localized biofilm disassembly and cell death, suggesting that biofilm detachment may be driving the release of cells for recolonization on other surfaces. For KCTC 11533, minimal fluorescence and scattered cells are observed at 24 h (Fig. 4M), suggesting slow initial growth. By 48 h (Fig. 4N), progression remains limited, with slight fluorescence and cell clustering increases. At 72 h (Fig. 4O), moderate fluorescence reflects the formation of a partially mature biofilm, though less dense than those of other strains. By 96 h (Fig. 4P), clusters with prominent red fluorescence mark biofilm aging, cell death, and detachment, reinforcing the cyclic nature of biofilm development where dead cells provide space or signaling for new biofilm formation.

The results from CLSM underscore the dynamic nature of biofilm development for each strain. The transition from initial attachment (24 h) to active growth (48 h), followed by maturation (72 h) and

subsequent detachment or degradation (96 h), reflects the natural biofilm lifecycle. The red fluorescence at 96 h signifies the cell death stage, facilitating the release of planktonic cells to form new biofilm colonies. The observed differences in fluorescence patterns, intensities, and structural organization among the four strains provide critical insights into the biofilm development process. Confocal microscopy unveiled marked disparities in biofilm architecture among ATCC 15467, ATCC 7966, KCTC 2358, and KCTC 11533. While ATCC 15467 and KCTC 11533 demonstrated delayed biofilm initiation followed by rapid maturation, resembling patterns observed by (Jayaraman, et al., 2024) in *A. hydrophila* strains, their subsequent architectural development diverged from previous findings.

SEM

The SEM images presented in Fig. 5 offered a detailed visualization of both individual cell morphology and biofilm structures for the four *A. hydrophila* strains—ATCC 15467, ATCC 7966, KCTC 2358, and KCTC 11533. Panels on the left side of the Fig. 5 (A, C, E, and G) depict the individual cells, while the right-side panels (B, D, F, and H) illustrate the corresponding biofilm formations. For ATCC 15467, Panel A shows well-defined, rod-shaped cells with distinct cellular boundaries, typical of *Aeromonas* morphology. The corresponding biofilm in Panel B reveals a

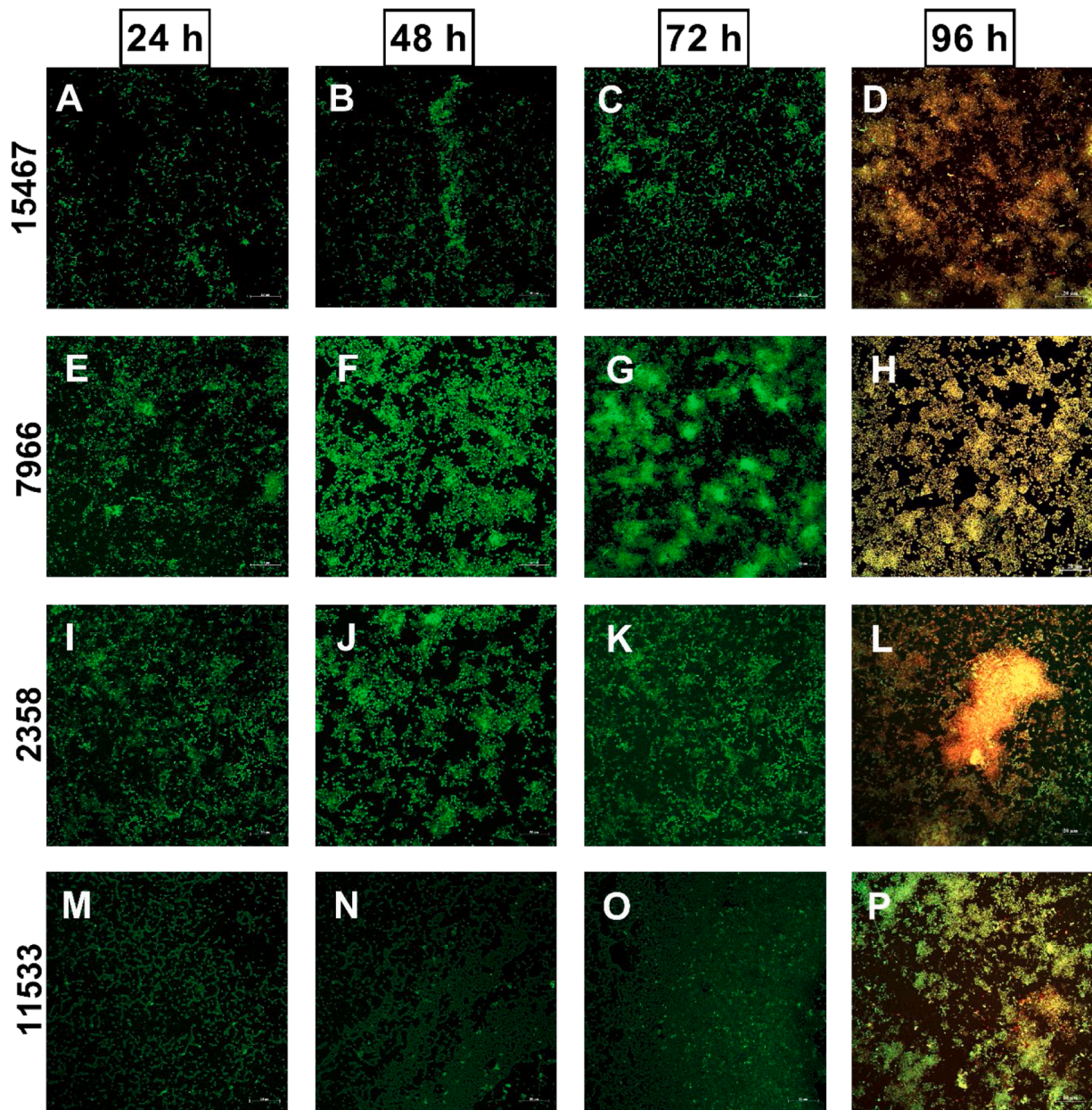


Fig. 4. Confocal images of four *A. hydrophila* strains ATCC 15467 (A-D), ATCC 7966 (E-H), KCTC 2358 (I-L), and KCTC (M-P).

densely packed, aggregated structure, indicating a strong biofilm-forming ability on PET surfaces. In contrast, ATCC 7966, depicted in Panel C, exhibits slightly elongated cells with smooth surfaces. The biofilm shown in Panel D is more dispersed, with visible ECM components, suggesting a well-organized biofilm. KCTC 2358 (Panel E) displays similarly shaped rod-like cells of consistent size with smooth surfaces. The biofilm formation in Panel F, however, is notably robust, with a large, rounded structure and cells embedded within a substantial ECM, indicating a highly developed biofilm. Lastly, KCTC 11533 (Panel G) consists of slightly larger and more robust cells. The biofilm in Panel H is complex, characterized by multiple layers and dense clusters of cells within a thick ECM, reflecting an advanced stage of biofilm maturation.

These SEM images underscore the biofilm-forming capabilities of all four *A. hydrophila* strains, each exhibiting distinct structural characteristics. The SEM images reveal that ATCC 15467 forms densely packed biofilms with well-defined rod-shaped cells, ATCC 7966 produces more dispersed biofilms with visible ECM components, KCTC 2358 creates robust biofilms with large, rounded structures, and KCTC 11533

develops complex, multi-layered biofilms with dense cell clusters. These variations in biofilm architecture—ranging from dense, compact formations to more complex, multi-layered structures—are consistent with previous studies (De Sousa, et al., 2015; Jahid, et al., 2014, 2013) that have highlighted the robust biofilm formation capabilities of each *A. hydrophila* strain.

Conclusion

This study highlights the strain-specific differences in biofilm formation, antibiotic resistance, motility, and gene expression among *A. hydrophila* strains ATCC 15467, ATCC 7966, KCTC 2358, and KCTC 11533. PET and SR surfaces were most conducive to biofilm formation, with ATCC 7966 exhibiting the highest biofilm density at 72 h, while HDPE demonstrated the lowest biofilm levels, indicating its potential as a biofilm-resistant material. The strains demonstrated notable resistance to multiple antibiotics, with specific agents remaining effective against certain strains. Motility assays identified KCTC 11533 as the most

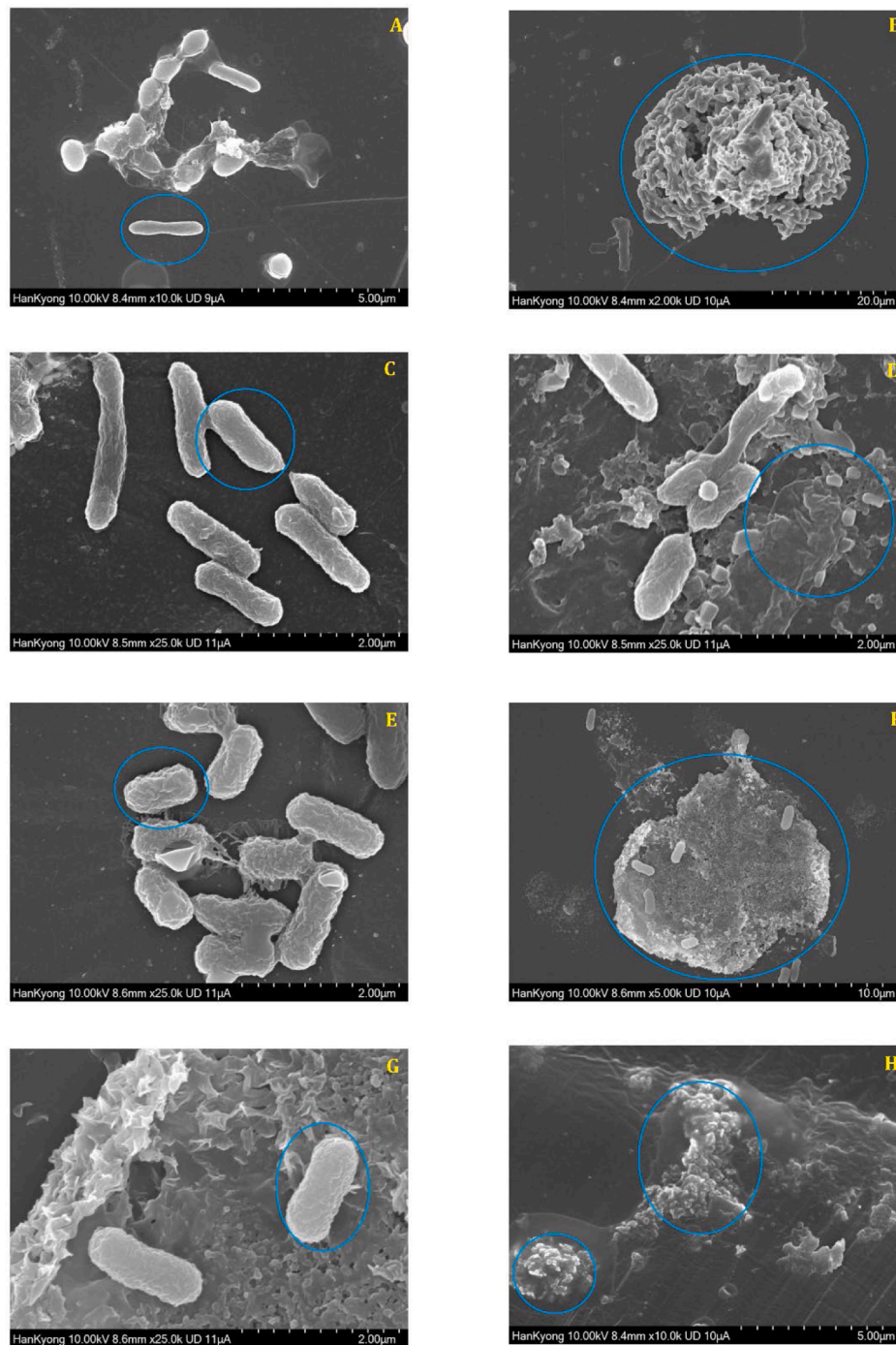


Fig. 5. FE-SEM images showing the morphological view of single cells (left column) and biofilm structures (right column) of *A. hydrophila* strains—ATCC 15467 (A, B); ATCC 7966 (C, D); KCTC 2358 (E, F); KCTC 11533 (G, H).

motile strain, exhibiting the highest swimming motility, while KCTC 2358 displayed superior swarming motility. Gene expression analysis revealed that SS enhanced *luxS* expression, while PET upregulated *ahyR*, promoting biofilm maturation. These findings underscore the critical influence of surface material on biofilm formation, resistance, and gene expression, providing valuable insights for designing strategies to mitigate biofilm formation and enhance food safety in processing environments.

Declaration of competing interest

There are no potential conflicts of interests.

Acknowledgements

This work was supported by the National Research Foundation of Korea (NRF) grant funded by the Korea government (MSIT) (RS202400339436) and also grant (21153MFDS605) from the Ministry of Food and Drug Safety in 2023.

References

Abd El-Ghany, W.A., 2023. A review on aeromoniasis in poultry: a bacterial disease of zoonotic nature. *J. Infect. Dev. Ctries.* 17, 1–9. <https://doi.org/10.3855/jidc.17186>.

- Akter, S., Rahman, M.A., Ashrafudoulla, M., Park, S.H., Ha, S.-D., 2025. Seafood and biofilm: mitigation strategies for food safety. *Food Control* 168, 110932. <https://doi.org/10.1016/j.foodcont.2024.110932>.
- Al-Amshawee, S., Yunus, M.Y.B.M., Lynam, J.G., Lee, W.H., Dai, F., Dakhlil, I.H., 2021. Roughness and wettability of biofilm carriers: a systematic review. *Environ. Technol. Innov.* 21, 101233. <https://doi.org/10.1016/j.eti.2020.101233>.
- Ali, F., Yao, Z., Li, W., Sun, L., Lin, W., Lin, X., 2018. In-Silico prediction and modeling of the quorum sensing LuxS protein and inhibition of AI-2 biosynthesis in aeromonas hydrophila. *Molecules* 23, 1–22. <https://doi.org/10.3390/molecules23102627>.
- Ashikur Rahman, M., Akter, S., Ashrafudoulla, M., Hasan Chowdhury, M.A., Uddin Mahamud, A.G.M.S., Park, S.H., Ha, S.-D., 2024. Insights into the mechanisms and key factors influencing biofilm formation by *Aeromonas hydrophila* in the food industry: a comprehensive review and bibliometric analysis. *Food Res. Int.* 175, 113671. <https://doi.org/10.1016/j.foodres.2023.113671>.
- Ashrafudoulla, M., Mevo, S.I.U., Song, M., Chowdhury, M.A.H., Shaila, S., Kim, D.H., Nahar, S., Toushik, S.H., Park, S.H., Ha, S.-D., 2023. Antibiofilm mechanism of peppermint essential oil to avert biofilm developed by foodborne and food spoilage pathogens on food contact surfaces. *J. Food Sci.* 88, 3935–3955. <https://doi.org/10.1111/1750-3841.16712>.
- Ashrafudoulla, M., Park, J., Toushik, S.H., Shaila, S., Ha, A.J.-w., Rahman, M.A., Park, S. H., Ha, S.-D., 2024a. Synergistic mechanism of UV-C and postbiotic of *Leuconostoc mesenteroides* (J.27) combination to eradicate *Salmonella* Thompson biofilm in the poultry industry. *Food Control* 164, 110607. <https://doi.org/10.1016/j.foodcont.2024.110607>.
- Ashrafudoulla, M., Yun, H., Ashikur Rahman, M., Jung, S.-J., Jie-Won Ha, A., Anamul Hasan Chowdhury, M., Shaila, S., Akter, S., Park, S.H., Ha, S.-D., 2024b. Prophylactic efficacy of baicalin and carvacrol against *Salmonella* Typhimurium biofilm on food and food contact surfaces. *Food Res. Int.* 187, 114458. <https://doi.org/10.1016/j.foodres.2024.114458>.
- Bahr, G., González, L.J., Vila, A.J., 2021. Metallo- β -lactamases in the age of multidrug resistance: from structure and mechanism to evolution, dissemination, and inhibitor design. *Chem. Rev.* 121, 7957–8094. <https://doi.org/10.1021/acs.chemrev.1c00138>.
- Bi, Z.X., Liu, Y.-J., Lu, C.P., 2007. Contribution of AhyR to virulence of aeromonas hydrophila J-1. *Res. Vet. Sci.* 83, 150–156. <https://doi.org/10.1016/j.rvsc.2007.01.003>.
- Busscher, H.J., Bos, R., van der Mei, H.C., 1995. Initial microbial adhesion is a determinant for the strength of biofilm adhesion. *FEMS Microbiol. Lett.* 128, 229–234. <https://doi.org/10.1111/j.1574-6968.1995.tb07529.x>.
- Chen, L., Wilksch, J.J., Liu, H., Zhang, X., Torres, V.V.L., Bi, W., Mandala, E., Cao, J., Li, J., Lithgow, T., Zhou, T., 2020. Investigation of LuxS-mediated quorum sensing in *Klebsiella pneumoniae*. *J. Med. Microbiol.* 69, 402–413. <https://doi.org/10.1099/jmm.0.001148>.
- CLSI, 2016. M45: Methods for Antimicrobial Dilution and Disk Susceptibility Testing of Infrequently Isolated or Fastidious. *Bacteria Clinical and Laboratory Standards Institute, Water, PA, USA*.
- De Sousa, J.P., De Oliveira, K.A.R., De Figueiredo, R.C.B.Q., De Souza, E.L., 2015. Influence of carvacrol and 1,8-cineole on cell viability, membrane integrity, and morphology of aeromonas hydrophila cultivated in a vegetable-based broth. *J. Food Prot.* 78, 424–429. <https://doi.org/10.4315/0362-028X.JFP-14-242>.
- Donlan, R.M., 2002. Biofilms: microbial life on surfaces. *Emerg. Infect. Dis.* 8, 881–890. <https://doi.org/10.3201/eid0809.020063>.
- Dueholm, M.S., Nielsen, S.B., Hein, K.L., Nissen, P., Chapman, M., Christiansen, G., Nielsen, P.H., Otzen, D.E., 2011. Fibrillation of the major curli subunit CsgA under a wide range of conditions implies a robust design of aggregation. *Biochemistry* 50, 8281–8290. <https://doi.org/10.1021/bi200967c>.
- Dula, S., Ajayebba, T.A., Ijbadeniya, O.A., 2021. Bacterial biofilm formation on stainless steel in the food processing environment and its health implications. *Folia Microbiol. (Praha)* 66, 293–302. <https://doi.org/10.1007/s12223-021-00864-2>.
- El-Hossary, D., Mahdy, A., Elariny, E.Y.T., Askora, A., Merwad, A.M.A., Saber, T., Dahshan, H., Hakami, N.Y., Ibrahim, R.A., 2023. Antibiotic resistance, virulence gene detection, and biofilm formation in aeromonas spp. isolated from fish and humans in Egypt. *Biology* 12, 421.
- Elhariry, H.M., 2011. Biofilm Formation by aeromonas hydrophila on green-leafy vegetables: cabbage and lettuce. *Foodborne Pathog. Dis.* 8, 125–131. <https://doi.org/10.1089/fpd.2010.0642>.
- Fernando, S.I.D., Judan Cruz, K.G., 2020. Ethnobotanical biosynthesis of gold nanoparticles and its downregulation of quorum sensing-linked AhyR gene in aeromonas hydrophila. *SN Appl. Sci.* 2, 570. <https://doi.org/10.1007/s42452-020-2368-1>.
- Grilo, M.L., Sousa-Santos, C., Robalo, J., Oliveira, M., 2020. The potential of *Aeromonas* spp. from wildlife as antimicrobial resistance indicators in aquatic environments. *Ecol. Indic.* 115, 106396. <https://doi.org/10.1016/j.ecolind.2020.106396>.
- Gu, H., Ren, D., 2014. Materials and surface engineering to control bacterial adhesion and biofilm formation: a review of recent advances. *Front. Chem. Sci. Eng.* 8, 20–33. <https://doi.org/10.1007/s11705-014-1412-3>.
- Gutell, R.R., Larsen, N., Woese, C.R., 1994. Lessons from an evolving rRNA: 16S and 23S rRNA structures from a comparative perspective. *Microbiol. Rev.* 58, 10–26. <https://doi.org/10.1128/mr.58.1.10-26.1994>.
- Hernould, M., Gagné, S., Fournier, M., Quentin, C., Arpin, C., 2008. Role of the AheABC efflux pump in aeromonas hydrophila intrinsic multidrug resistance. *Antimicrob. Agents Chemother.* 52, 1559–1563. <https://doi.org/10.1128/aac.01052-07>.
- Jahid, I.K., Han, N., Ha, S.-D., 2014. Inactivation kinetics of cold oxygen plasma depend on incubation conditions of *Aeromonas hydrophila* biofilm on lettuce. *Food Res. Int.* 55, 181–189. <https://doi.org/10.1016/j.foodres.2013.11.005>.
- Jahid, I.K., Lee, N.-Y., Kim, A., Ha, S.-D., 2013. Influence of glucose concentrations on biofilm formation, motility, exoprotease production, and quorum sensing in aeromonas hydrophila. *J. Food Prot.* 76, 239–247. <https://doi.org/10.4315/0362-028X.JFP-12-321>.
- Jahid, I.K., Mizan, M.F.R., Myoung, J., Ha, S.-D., 2018. *Aeromonas hydrophila* biofilm, exoprotease, and quorum sensing responses to co-cultivation with diverse foodborne pathogens and food spoilage bacteria on crab surfaces. *Biofouling* 34, 1079–1092. <https://doi.org/10.1080/08927014.2018.1519069>.
- Janda, J.M., Abbott Sharon, L., 2010. The Genus *Aeromonas*: taxonomy, Pathogenicity, and Infection. *Clin. Microbiol. Rev.* 23, 35–73. <https://doi.org/10.1128/cmr.00039-09>.
- Jayaraman, S., Rajendran, N., Kannan, M.A., Ramasamy, T., 2024. Quercetin disrupts biofilm formation and attenuates virulence of *Aeromonas hydrophila*. *Arch. Microbiol.* 206, 326. <https://doi.org/10.1007/s00203-024-04034-z>.
- Kearns, D.B., 2010. A field guide to bacterial swarming motility. *Nat. Rev. Microbiol.* 8, 634–644. <https://doi.org/10.1038/nrmicro2405>.
- Krumpalman, P.H., 1983. Multiple antibiotic resistance indexing of *Escherichia coli* to identify high-risk sources of fecal contamination of foods. *Appl. Environ. Microbiol.* 46, 165–170. <https://doi.org/10.1128/aem.46.1.165-170.1983>.
- Lackner, S., Holmberg, M., Terada, A., Kingshott, P., Smets, B.F., 2009. Enhancing the formation and shear resistance of nitrifying biofilms on membranes by surface modification. *Water Res.* 43, 3469–3478. <https://doi.org/10.1016/j.watres.2009.05.011>.
- Lejeune, P., 2003. Contamination of abiotic surfaces: what a colonizing bacterium sees and how to blur it. *Trends Microbiol.* 11, 179–184. [https://doi.org/10.1016/s0966-842x\(03\)00047-7](https://doi.org/10.1016/s0966-842x(03)00047-7).
- Livak, K.J., Schmittgen, T.D., 2001. Analysis of relative gene expression data using real-time quantitative PCR and the 2⁻ $\Delta\Delta$ CT method. *Methods* 25, 402–408. <https://doi.org/10.1006/meth.2001.1262>.
- Lv, J., Li, Y., Zhou, K., Guo, P., Liu, Y., Ding, K., Li, K., Zhong, C., Xiao, B., 2020. Force spectra of single bacterial amyloid CsgA nanofibers. *RSC Adv.* 10, 21986–21992. <https://doi.org/10.1039/D0RA02749A>.
- Ma, J., Zhao, H., Mo, S., Li, J., Ma, X., Tang, Y., Li, H., Liu, Z., 2023. Acquisition of type I methyltransferase via horizontal gene transfer increases the drug resistance of *Aeromonas veronii*. *Microb. Genom.* 9, 1–13. <https://doi.org/10.1099/mgen.0.001107>.
- Martins, D.L., Cabral, A.N., Winter, H.C.L., Mariotto, S., Nascimento, E., Faria, R.A.P.G. d., Martins, E.d.L., Ritter, D.O., Lanzarin, M., 2023. Resistance of *Aeromonas hydrophila* isolates to antimicrobials and sanitizers. *Ciência Rural* 53, e20220256.
- Mitik-Dineva, N., Wang, J., Truong, V.K., Stoddart, P., Malherbe, F., Crawford, R.J., Ivanova, E.P., 2009. *Escherichia coli*, *Pseudomonas aeruginosa*, and *Staphylococcus aureus* attachment patterns on glass surfaces with nanoscale roughness. *Curr. Microbiol.* 58, 268–273. <https://doi.org/10.1007/s00284-008-9320-8>.
- O'Toole, G.A., Kolter, R., 1998. Flagellar and twitching motility are necessary for *Pseudomonas aeruginosa* biofilm development. *Mol. Microbiol.* 30, 295–304. <https://doi.org/10.1046/j.1365-2958.1998.01062.x>.
- Rahman, M.A., Akter, S., Khan, M.M., Rahman, M.K., 2019. Relation between aquaculture with fish disease & health management: a review note. *Bangladesh J. Fisher.* 31, 253–260.
- Rahman, M.A., Ashrafudoulla, M., Akter, S., Park, S.H., Ha, S.-D., 2023. Probiotics and biofilm interaction in aquaculture for sustainable food security: a review and bibliometric analysis. *Crit. Rev. Food Sci. Nutr.* 64 (33), 1–17. <https://doi.org/10.1080/10408398.2023.2249114>.
- Rather, M.A., Gupta, K., Mandal, M., 2021. Microbial biofilm: formation, architecture, antibiotic resistance, and control strategies. *Braz. J. Microbiol.* 52, 1701–1718. <https://doi.org/10.1007/s42770-021-00624-x>.
- ROSSOLINI, G.M., WALSH, T., AMICOSANTE, G., 1996. The *Aeromonas* metallo- β -lactamases: genetics, enzymology, and contribution to drug resistance. *Microb. Drug Resist.* 2, 245–252.
- Sehree, M.M., Abdullah, H.N., Jasim, A.M., 2022. Comparison of phenotypic and genotypic assays of biofilm formation in *A. baumannii* isolates based on gold standard method and related antibiotic resistance. *Gene Rep.* 27, 101575. <https://doi.org/10.1016/j.genrep.2022.101575>.
- Vickery, K., Pajkos, A., Cossart, Y., 2004. Removal of biofilm from endoscopes: evaluation of detergent efficiency. *Am. J. Infect. Control.* 32, 170–176. <https://doi.org/10.1016/j.ajic.2003.10.009>.
- Wadhwa, N., Berg, H.C., 2022. Bacterial motility: machinery and mechanisms. *Nat. Rev. Microbiol.* 20, 161–173. <https://doi.org/10.1038/s41579-021-00626-4>.
- Wang, Y., Liu, B., Grenier, D., Yi, L., 2019. Regulatory Mechanisms of the LuxS/AI-2 System and Bacterial Resistance. *Antimicrob. Agents Chemother.* 63, 1–12. <https://doi.org/10.1128/aac.01186-01119>.
- Yan, Z., Huang, M., Melander, C., Kjellerup, B.V., 2020. Dispersal and inhibition of biofilms associated with infections. *J. Appl. Microbiol.* 128, 1279–1288. <https://doi.org/10.1111/jam.14491>.
- Zanzan, M., Ezzaky, Y., Achemchem, F., Hamadi, F., Amzil, K., Latrache, H., 2024. Bacterial biofilm formation on stainless steel: exploring the capacity of *Enterococcus* spp. isolated from dairy products on AISI 316 L and AISI 304 L surfaces. *Biologia (Bratisl)* 79, 1539–1551. <https://doi.org/10.1007/s11756-024-01630-8>.
- Zottola, E.A., Sasahara, K.C., 1994. Microbial biofilms in the food processing industry—should they be a concern? *Int. J. Food Microbiol.* 23, 125–148. [https://doi.org/10.1016/0168-1605\(94\)90047-7](https://doi.org/10.1016/0168-1605(94)90047-7).